CHEMICAL PHYSICS

Selective isomer emission via funneling of exciton polaritons

Sitakanta Satapathy[1], Mandeep Khatoniar[1,2], Divya K. Parappuram[3], Bin Liu[4], George John[3]*, Johannes Feist[5]*, Francisco J. Garcia-Vidal[5]*, Vinod M. Menon[1,2]*

Polaritons in organic systems has shown the potential to modify chemical properties and to mediate long-range energy transfer between individual chromophores, among other capabilities. Here, we demonstrate that strong coupling and formation of organic exciton-polaritons can be used to selectively tune the isomer emission of organic molecules. By taking advantage of their delocalized and hybrid character, polaritons emerging in the strong coupling regime open a new relaxation pathway that allows for an efficient funneling of the excitation between the molecular isomers. We implement this by strong coupling to *trans*-DCS (*E*-4-dimethylamino-4′cyanostilbene) molecules, which present two isomers in different amounts when immersed in a polymer matrix. Thanks to this new relaxation pathway, the photoexcitation that is first shared by the common polaritonic mode is then selectively funneled to the excited states of one of the isomers, recognizing pure emission from the isomeric states that do not contribute to emission under normal conditions.

INTRODUCTION

The phenomenon by which some molecules present two or more different arrangements of their atoms in space that are compatible with their molecular formula is called isomerism, which is ubiquitous in organic chemistry. A feasible way to trigger an interplay between isomers is the absorption of an ultraviolet (UV) photon, which allows for operating within the excited states of the isomers. While the photophysical properties of isomers are of great significance in the field of organic photovoltaics (*1*), optoelectronics (*2*), and many biochemical events (*3*), it is the correct choice and purity of the photoisomer luminescence that plays a decisive role in being favored or disfavored for a particular application.

During the past 10 years, substantial experimental and theoretical progress has been made to demonstrate the potential use of strong light-matter coupling for both modifying molecular energy landscapes (*4*–*11*) and enhancing energy transfer in donor-acceptor molecular systems (*12*–*19*), among other capabilities (*20*). In general, strong coupling emerges when a collection of quantum emitters is placed within an optical cavity and the coherent energy exchange between the excitons in the emitters and photons inside the cavity is faster than the loss mechanisms in the combined system (*21*). The most important fingerprint of strong coupling is the emergence of new hybrid light-matter states, usually named polaritonic states, which inherit interesting properties from their two constituents, light and matter, and have a delocalized character. Owing to their large dipole moments, high densities and tightly bound Frenkel excitons, organic materials (*22*–*24*) hold enormous potential in the context of strong coupling since they provide extremely robust polaritonic modes

under ambient conditions with large Rabi splitting up to 1 eV. In addition to the emergence of polaritonic states, collective strong coupling also results in the formation of a manifold of dark states that cannot be directly excited with light but plays an important role in the excitation dynamics (*10*).

In this work, we introduce a route to select isomer luminescence by also using the phenomenon of collective strong light-matter coupling. The mechanism relies on the funneling of the excitation through the collective polaritonic mode, taking advantage of its delocalized character. By choosing an organic molecule in which the two isomers display a very similar absorption spectrum, the resulting polaritonic mode has contributions from the two excited states of the isomers that are present in the sample. If the two isomers present a distinct luminescence, we show how the initial photoexcitation that has been stored in the common polaritonic mode can be efficiently funneled to one of the excited states of the isomer if the Rabi splitting is large enough to surpass the energy difference between those states. Thanks to this new energy pathway, it is then feasible to reshape the luminescence spectrum of the organic material by favoring the emission from one of the isomers for a particular application.

RESULTS

Figure 1A shows the chemical structure of the molecule used in our study, *trans*-DCS (*E*-4-dimethylamino-4′cyanostilbene). This molecule is a highly conjugated donor-acceptor system that undergoes an intramolecular charge transfer (ICT) process following UV excitation [see Fig. 1A] (*25*). Both the high conjugation and the ICT character of the excited state induce a large increase of the molecular dipole moment, and consequently, this organic molecule presents a large Stokes shift and a substantial two-photon activity. These two properties make *trans*-DCS potentially relevant for several applications, such as two-photon excited fluorescence microscopy (*26*, *27*), three-dimensional optical data storage (*28*), and biological caging studies (*29*). Schematic representations of the ground and excited states of *trans*-DCS molecules are shown in Fig. 1D. These molecules can form two different isomers when immersed in a polymer film: the planar (P) and nonplanar (NP) states (*30*–*33*). To be used

[1]Department of Physics, Center for Discovery and Innovation, City College of New York, City University of New York, 85 St. Nicholas Terrace, New York, NY 10031, USA. [2]PhD Program in Physics, The Graduate Center, City University of New York, 365 5th Avenue, New York, NY, 10016, USA. [3]Department of Chemistry, Center for Discovery and Innovation, City College of New York, City University of New York, 85 St. Nicholas Terrace, New York, NY 10031, USA. [4]Department of Electrical Engineering and Computer Science, University of Michigan, Ann Arbor, Michigan 48109, USA. [5]Departamento de Física Teórica de la Materia Condensada and Condensed Matter Physics Center (IFIMAC), Universidad Autónoma de Madrid, 28049 Madrid, Spain.
*Corresponding author. Email: gjohn@ccny.cuny.edu (G.J.); johannes.feist@uam.es (J.F.); fj.garcia@uam.es (F.J.G.-V.); vmenon@ccny.cuny.edu (V.M.M.)
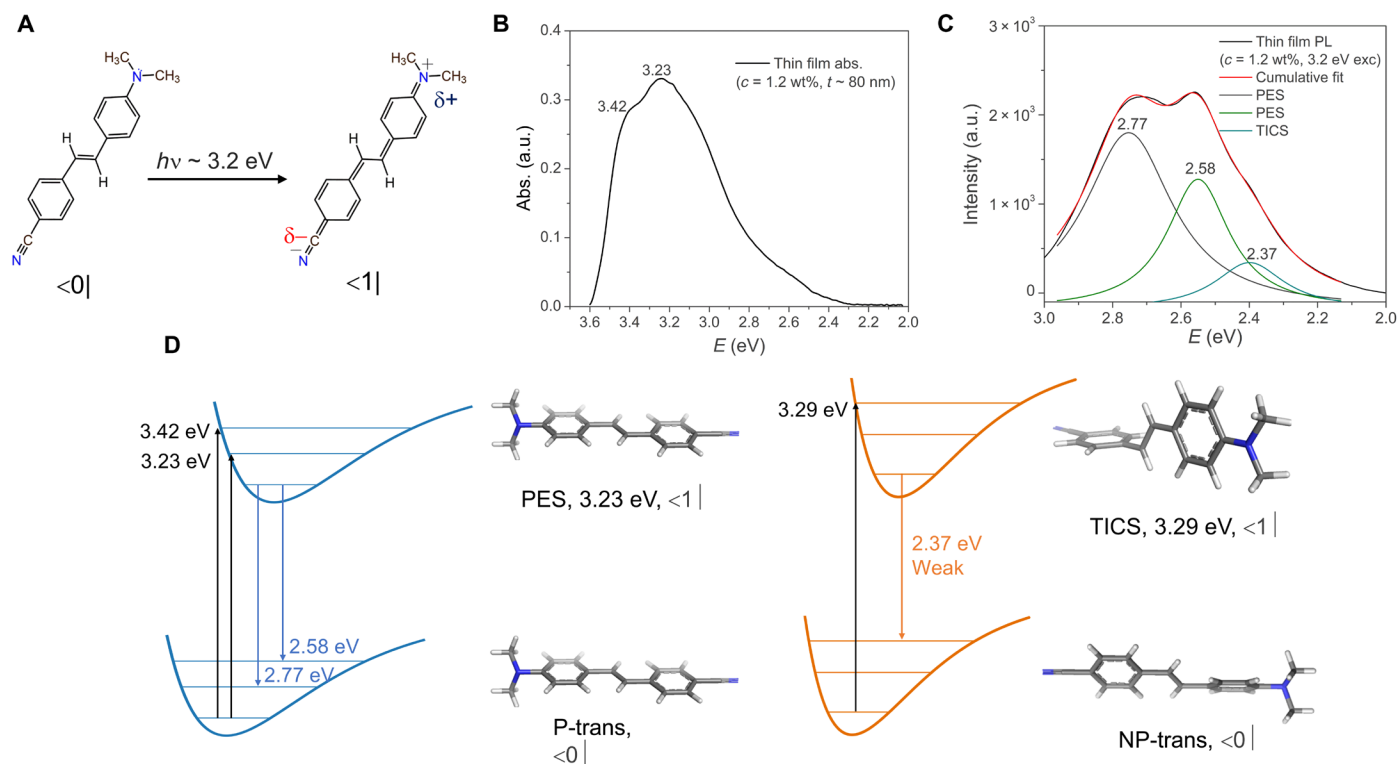
Fig. 1. Optical characterization of the thin film sample. (**A**) The ground (|0>) and the excited ICT state (|1>) chemical structures of *trans*-DCS, (**B**) absorption and (**C**) PL plots (the deconvoluted peaks assign the spectral weights for the respective PES and TICS exciton emission), and (**D**) schematic comparing the respective absorption and emission energies of the ground (P and NP) and excited state (PES and TICS) configurations of DCS (c = 1.2 wt%) thin film (~80 nm) over Ag. a.u., arbitrary units.

as a reference system, the first set of samples are fabricated by using thin (~80 nm) films of DCS molecules that are spin-coated from the anisole solution of polymethyl methacrylate (PMMA) and deposited on silver thin (~100 nm) films after that. Details of the film fabrication steps are described in Materials and Methods. Figure 1 compares the absorption (Fig. 1B) and photoluminescence (PL) spectrum (Fig. 1C) of this structure. DCS layers present a broad absorption spectrum, with its maximum centered at 3.23 eV (X_1) and a weak vibrational signature at 3.42 eV (X_2). The PL spectrum displays two maxima at 2.77 and 2.58 eV and a shoulder at 2.37 eV. It is worth commenting that this weak PL feature appears only at high concentrations [≥1 weight % (wt%)], as shown in fig. S1. As discussed below, this feature corresponds to photon emission from an isoenergetic twisted ICT excited state (TICS) of the molecule (*34, 35*), implying that the fraction of NP-trans isomers in our DCS films increases with concentration. Unlike the PL spectrum, absorption does not present a notable change when the molecular concentration is varied (see fig. S1).

Previous studies have used Raman spectroscopy as a tool to characterize these two isomers, reporting that the less common NP isomer is usually formed when DCS molecules are placed in rigid polymeric environments (*31–33*). In the NP configuration, the two phenyl rings are oriented at an angle of ~30° with respect to each other around the central ethylenic double bond. In the Raman signal, this NP-trans isomer differs from the corresponding P-trans one only by its ethylenic —CH vibrations, resulting in an energy shift of the corresponding Raman mode from 874 cm^{-1} (P-trans) to 967 cm^{-1} (NP-trans). Confocal Raman spectroscopy measurements

of DCS films with varying concentrations deposited on silver films, as shown in fig. S3, confirm that these two molecular configurations are present in our samples. Moreover, when comparing the dependence of intensity of the Raman modes on molecular concentration, a distinct behavior for the P-trans and NP-trans signatures is observed. It is found that both configurations are present in very different amounts within the polymer film, with the P-trans isomer being the dominant one for all concentrations while the NP-trans isomer being detected only at high enough concentrations. To complete the picture, our density functional theory (DFT)–calculated Raman spectrum for the NP-trans configuration, as rendered in fig. S4, also agrees with our experimental results. With respect to their excited states, the planar excited state (PES) and TICS isomers are formed after photoexcitation of P-trans and NP-trans ground states of DCS, respectively. Our DFT calculations predict negligible energy difference in absorption energies for the two configurations with the NP-trans being slightly higher in energy (ΔE_{abs} ~ 30 meV) with respect to the P-trans (see fig. S5), explaining why the absorption spectrum does not present additional features associated with the NP-trans isomer as molecular concentration is increased, in contrast to the PL spectrum.

Now, we analyze how the absorption, PL, and Raman spectra of the molecular film changes when it is placed inside a Fabry-Perot (FP) cavity, which consists of two silver mirrors sandwiching ~80-nm-thick DCS film. As in the reference system, DCS layers with varying molecular concentrations (0.2 to 1.2 wt%) are first spin-coated over a 100-nm-thick silver film, which will act then as the bottom mirror of the FP cavity. After that, another 30-nm-thick

silver film is deposited on top to close the cavity (see Materials and Methods for more details). The geometrical parameters of the structure are chosen such that the energy of the FP cavity mode almost coincides with the DCS absorption maximum, 3.23 eV.

A representative angle-resolved (20° to 80°) reflection spectrum of one of the fabricated microcavities is displayed in Fig. 2A, obtained for a DCS concentration of 1.2 wt% and transverse magnetic (TM) incident light polarization. The reflection energy data measured at various incident angles (fig. S6) are overlaid on the simulation results to show the dispersion relation in Fig. 2A. The three minima for each incident angle are a fingerprint of the emergence of strong coupling and correspond to the excitation of the upper polariton (UP), middle polariton (MP), and lower polariton (LP) states. From a fit based on a three-coupled oscillator model that accounts for the coupling between the FP cavity mode and DCS excitons X_1 [3.23 eV, full width at half maximum (fwhm) ~ 0.24 eV] and X_2 (3.42 eV, fwhm ~ 0.10 eV), we can determine light-matter coupling strengths of g_1 ~ 0.26 eV and g_2 ~ 0.06 eV, respectively. This leads to a total Rabi splitting of Ω_R ~ 0.64 ± 0.05 eV between LP and UP (the two modes with significant contributions from the cavity mode). The dependence of the Rabi splitting energy on molecular concentration is shown in fig. S7, implying that strong coupling is achieved for molecular concentrations higher than 0.8 wt%.

The PL spectrum for the strongly coupled cavity sample does not follow the dispersion of the LP mode (see Fig. 2B), although the excitation energy coincides spectrally with that of the LP mode (2.8 eV). Instead, it shows an almost nondispersive emission at 2.37 eV, indicating that this emission could come from the TICS dark states of the NP-trans configuration of the molecule. Figure 2 (C and D) compares the excitation energy–dependent PL spectra of DCS ($c = 1.2$ wt%) for the reference system and for the FP cavity case, respectively. As discussed above, the bare molecular film at high concentrations is characterized by an intense PES photon emission at 2.77 and 2.58 eV and a weak (for high energy excitation) to almost negligible (for low energy excitation) TICS emission at 2.37 eV. This evolution of the TICS emission is attributed to the low concentration of TICS isomeric states (with respect to PESs) in the sample, which need to be pumped higher in energy to fluoresce and then contribute to the broader tail of the PL intensity. As a difference, the PL spectrum in the strong coupling regime presents a more abrupt dependence on the excitation energy. Exciting the cavity sample close to the LP resonance (2.8 eV) results in a well-resolved PL signal coming from the TICS and no photon emission resulting from the PES. However, pumping more and more closely to the uncoupled exciton resonances at higher energies (>2.8 eV) provokes a broadening of the spectral profile, revealing emission from both PES and TICS. No angle-dependent PL response from the cavity samples is observed in this case either. This behavior is consistent with previous experimental observations for strongly coupled organic molecules that present a very large Stokes shift (36).
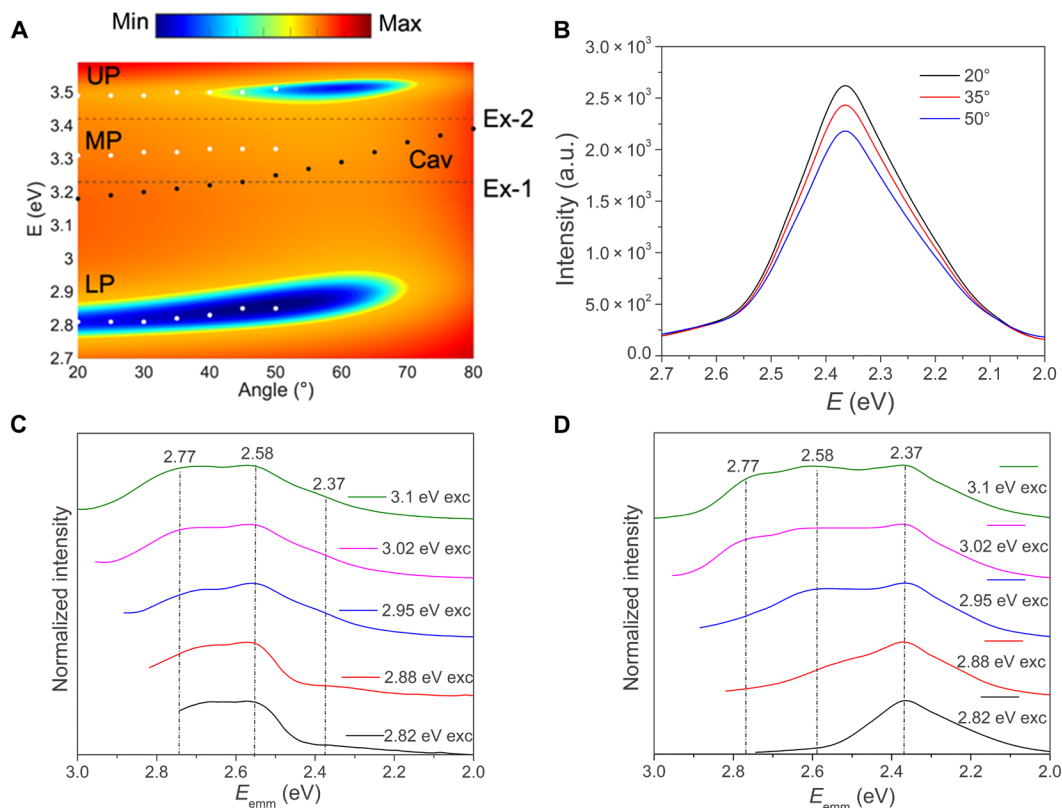

Fig. 2. Optical characterization and excitation pump–dependent PL of the cavity sample. (A) Angle-dependent reflection (TM polarization, 20° to 80°) data for a strongly coupled DCS cavity sample (white filled circles denote the measured polariton dispersion, while black circles and dashed lines indicate the bare cavity and exciton dispersion data, overlaid on the simulation results, respectively), **(B)** Angle-resolved PL from the strongly coupled cavity sample for an excitation energy of ~2.8 eV and normalized excitation energy–dependent PL spectra comparison for the **(C)** bare molecular films and **(D)** strongly coupled cavities of DCS ($c = 1.2$ wt%).

To elucidate the physical origin of the distinct behavior observed for strongly coupled samples, Fig. 3 (A to F) presents the evolution of the cavity PL spectrum as a function of the molecular concentration, varying from the weak ($c < 0.8$ wt%) to the strong ($c > 0.8$ wt%) coupling regime, for a fixed value of the excitation energy (3.2 eV), close to the bare exciton resonance (3.23 eV). PL spectra for the cavity samples at low concentrations (0.2 to 0.6 wt%) reveal features almost identical to those observed in the reference system (see fig. S2) for the same concentrations: two maxima at 2.77 and 2.58 eV, which correspond to emission from the excited state of the planar configuration, and no signatures of the TICS isomer. However, at higher concentrations (0.8 to 1.2 wt%), PL spectra show a complete modulation of emission spectral weights with contributions from the excited states of the two isomers: intense emission from TICS excitons at 2.37 eV along with weaker spectral features from PES excitons, just the opposite to what is observed for the reference system at the same concentrations, in which the PES peaks are always the dominant feature (see Fig. 1C).

In addition, as shown in Fig. 3 (G to I), the weak PL features from the PES excitons become negligible when the cavity is pumped close to the LP resonance (~2.8 eV). Although we cannot monitor the 2.77-eV emission from the PESs because it is too close in energy to the pump beam, the negligible emission at 2.58 eV (vibronic feature also coming from PESs) seems to indicate that the excitation has a very minor contribution from PESs in this case. Accompanying the disappearance of PES features in the PL spectrum, the corresponding PL peak at 2.37 eV largely increases with concentration. Although some of the increase is associated with just the presence of more NP-trans molecules and, thus, the availability of more TICSs (notice that TICS emission also increases with concentration in DCS bare molecular films, being nevertheless much smaller than that coming from PESs, as shown in fig. S2), most of the increase observed must come from another source as TICS emission is always greater than that coming from PESs, irrespective of the excitation energy used. Therefore, our results imply that, when the system enters the strong coupling regime, a new relaxation pathway is opened
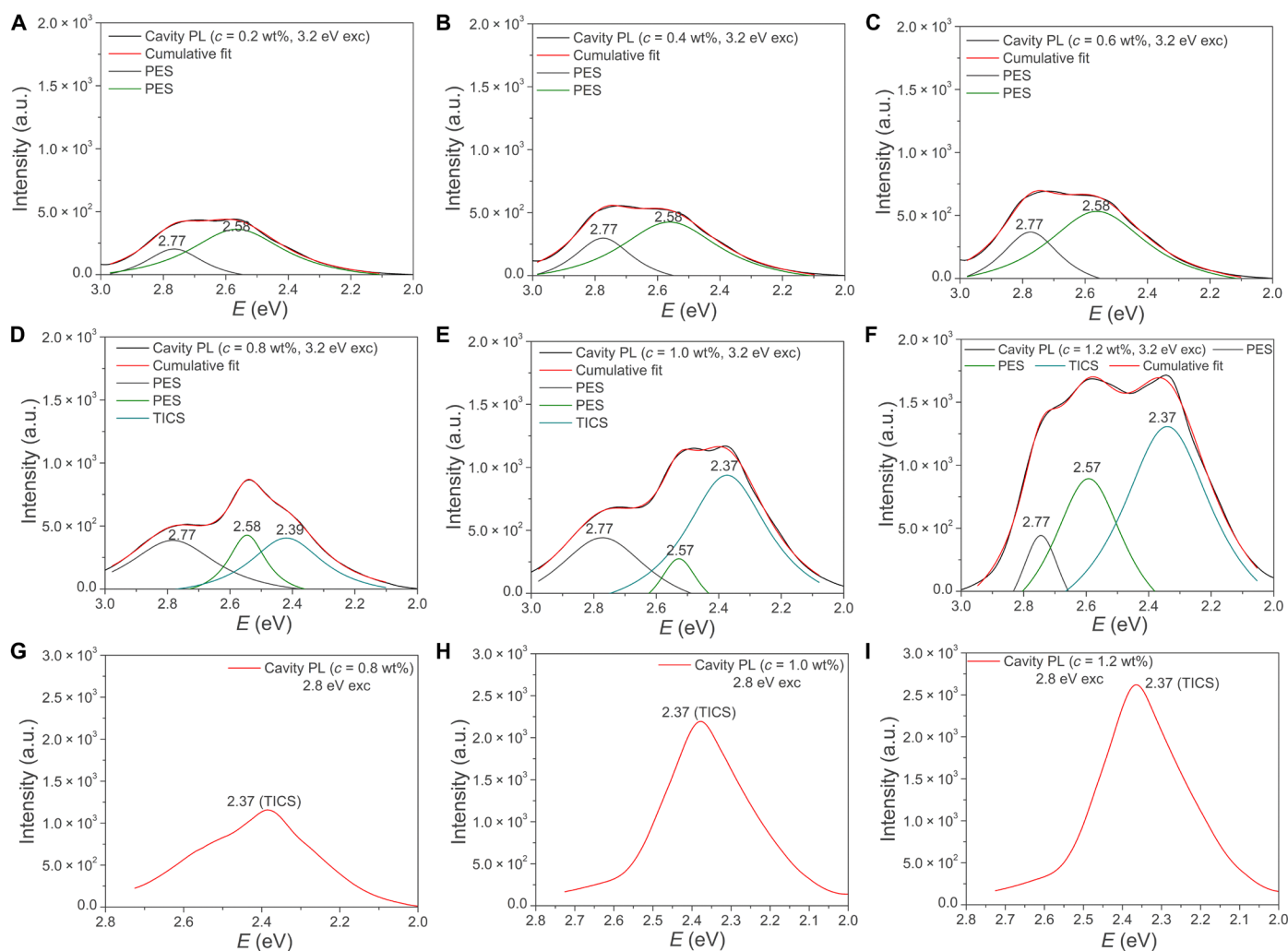

Fig. 3. Concentration-dependent PL of the cavity sample. Comparison of PL spectra for the cavity samples with varying concentrations for (**A**) 0.2 wt%, (**B**) 0.4 wt%, (**C**) 0.6 wt%, (**D**) 0.8 wt%, (**E**) 1.0 wt%, and (**F**) 1.2 wt% pumped close to the exciton resonance (~3.2 eV). PL spectra comparison only for the strongly coupled cavity samples with varying concentrations for (**G**) 0.8 wt%, (**H**) 1.0 wt%, and (**I**) 1.2 wt% pumped close to respective LP resonances (~2.8 eV).

that allows for an efficient excitation transfer from the LP mode to the TICS isomer, which becomes the dominant one when the excitation energy is resonant with the LP mode.

To further confirm that an exciton polariton funneling-type mechanism is responsible for the emission intensity enhancement from the TICS isomer and exclude the possibility of any polariton-induced photochemical change, we have carried out extensive concentration-dependent confocal Raman measurements on the cavity samples following their PL measurements and compared them with those for the corresponding bare molecular films (fig. S8 and S9). Figure 4 (A and B) shows the concentration-dependent increase of ethylenic–CH Raman modes (967 cm^{-1}) for the NP-trans isomer for the bare molecular films and cavity samples, respectively. In both cases, a nonlinear Langmuir type increase in Raman intensities for the 967-cm^{-1} peak is observed with saturation of Raman photons at higher concentrations. The origin of Langmuir curves in Raman spectra of organic systems have been discussed in previous reports (37, 38). The rise in the signal intensities occurring at different concentrations for the bare film and the cavity could be attributed to differences in the sample preparation inside and outside cavity, leading to different aggregation/assembly behaviors of DCS. As discussed previously, the NP-trans isomer is the ground state associated with the TICS excitons and is expected to undergo a population change following the TICS emission increase under the condition of a cavity-induced photochemical change (9, 11). However, the 967-cm^{-1} Raman mode enhancement as a function of concentration follows an almost identical trend, displaying approximately sixfold increase for both the bare molecular films and cavity samples. This suggests that there is no change in ground state isomerism induced by strong coupling, which is consistent with previous reports (5).

Figure 4C shows a sketch of the energetics in the strong coupling regime. The cavity mode (in the center) is close to resonant with the dominant transitions in both the P-trans and NP-trans isomers. The two optically active polaritons (LP and UP) are thus formed from the cavity mode and the vibrational levels that are visible in the absorption spectrum in both the PES and TICS (indicated by dashed arrows). Because of the energetics of the system, the lowest polariton becomes close in energy with the (optically dark) lowest vibrational level of the TICS accessed from the NP-trans isomer. This implies that vibration-mediated incoherent excitation transfer processes (indicated by the wavy green arrow) from the LP to the dark-state manifold corresponding to this lowest TICS level are highly efficient, following Kasha's rule that has been found to be also operative for strongly coupled systems (15, 36, 39). At the same time, vibration-mediated exciton transfer to the PESs becomes energetically forbidden and thus strongly suppressed. The delocalized LP
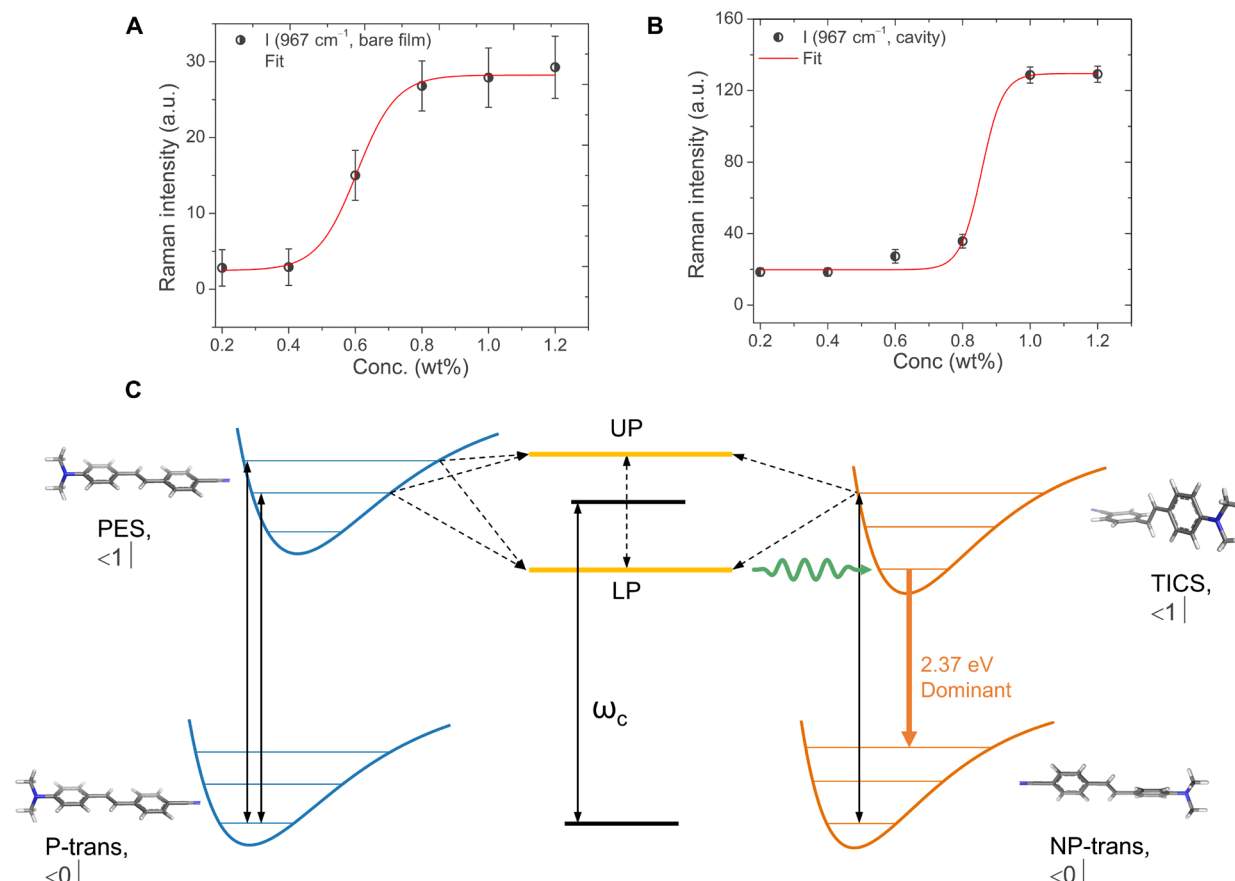

Fig. 4. Concentration-dependent Raman spectra of the cavity sample and schematic summarizing the polariton funneling mechanism. Comparison of concentration-dependent Raman (2.33 eV exc) intensities for the 967-cm^{-1} peak collected from the DCS film over (**A**) 100-nm Ag and (**B**) in microcavity following PL measurements. (**C**) Schematic describing the energy level alignments of the respective PESs and the polariton-induced energy funneling mechanism that transfer excitations from PES to TICS isomers of DCS molecules in cavities.

thus effectively acts as a funnel that can exploit the strong absorption of the dominant P-trans isomer but transfers a significant fraction of the excitations to localized molecular excitations in the TICS and consequently makes emission from the TICS the dominant radiative emission channel. As a difference from previous demonstrations of cavity-enhanced energy transfer processes in which the excitation is always carried out by the polaritonic states of the strongly-coupled system (*12–14, 16–19*), here, the mechanism uses the manifold of molecular dark states as the final emissive mode. The delocalized polaritonic state is only used to store first the excitation energy that is then transferred to the dark states. As a result, this funneling process is much faster than pure polariton-assisted transfer mechanisms because of the huge density of dark states when compared to polaritonic ones. We also note that since only excitations, not electrons, are exchanged between the different isomers, only "relative" (excitation) energies play a role, not the "absolute" (orbital) energies.

DISCUSSION

ICT active molecular isomers are donor-acceptor dyadic systems that find extensive use in the field of organic optoelectronics and molecular nonlinear optics. However, the success of the overall application is defined by the choice and purity of isomer emission. First, we have demonstrated strong coupling of a highly conjugated ICT active molecule, DCS, resulting in Rabi splitting energies up to $\Omega_R = 0.64 \pm 0.05$ eV (~19.8% of the total exciton energy). Our experiments also point to the emergence of a directional polariton energy transfer pathway in between the two photoisomers (PES and TICS) of DCS (*E*-4-dimethylamino-4′cyanostilbene) molecules, which are present in different amounts inside the cavity. This funneling process becomes more and more effective when the Rabi splitting is increased, and the optical pumping is close to the LP resonance, resulting in a complete spectral weight modulation and significant brightening of pure TICS exciton emission. The realization of TICS exciton emission in the strong coupling regime undergoes a significant intensity enhancement with respect to lowering of LP energy levels, suggesting an effective directional funneling of the energy associated with a delocalized LP onto the TICSs. On the other hand, concentration-dependent Raman investigations for the cavity samples confirm no change in ground state population as a function of strong coupling and thus reject the possibility of any polariton-induced photochemical change.

In the general context of cavity-induced modification of chemical and material properties, our contribution offers a new strategy toward successful harvesting/funneling of polariton energy to access desirable excited states of potential relevance in the field of organic photovoltaics, optoelectronics, and photobiological reactions. Through judicious choice of molecular systems and cavity design, our strategy could potentially be used in other scenarios, such as excited state induced proton transfer, electron transfer, and photooxidation reactions in photovoltaics.

MATERIALS AND METHODS
Synthesis
The synthesis of DCS is carried out in two steps as described below:

1) Synthesis of diethyl (4-cyanobenzyl)phosphonate. 4-cyanobenzyl bromide (5.1 mmol) and triethyl phosphite (6.12 mmol) were placed in a round-bottom flask. The reaction mixture was heated to 130°C for 1 hour and then cooled to room temperature. The remaining triethyl phosphite was removed under vacuum. The product was used for the next step without further purification [yield: 90 to 95%; 1H Nuclear Magnetic Resonance (NMR) [CDCl$_3$, 500 MHz, tetramethylsilane] δ (parts per million): 7.61 (d, 2H, ArH), 7.42 (d, 2H, ArH), 4.08 (m, 4H, —OCH$_2$—), 3.20 (s, 2H, —CH$_2$P—), and 1.15 (t, 6H, —CH$_3$)].

2) Synthesis of DCS. NaH (520 mg; 0.0216 mol) is added to a solution of 2.6 g (0.0108 mol) of phosphonate in 13 ml of *N,N′*-dimethylformamide. After 30 min, 3 g (0.0201 mmol) of *p*-dimethyl-aminobenzaldehyde is added, and the mixture is stirred overnight at 40°C. Then, the solution is poured on water and extracted with dichloromethane. The organic layer was washed with brine, dried over Na$_2$SO$_4$, and concentrated to give the crude product, which was further purified by column chromatography over silica gel with CH$_2$Cl$_2$ and gives DCS as yellow solid in 87% yield [1H NMR (dimethyl sulfoxide, 500 MHz): δ (parts per million): 7.75 (m, 4H, ArH), 7.49 (d, 2H, ArH), 7.38 (d, 1H, vinylic H), 7.07 (d, 1H, vinylic H), 6.75 (d, 2H, ArH), and 2.96 (s, 6H, —CH$_3$)].

Sample preparation
DCS precursor solution is obtained by dissolving about 0.2 to 1.2 wt% of DCS in 0.8 ml of commercial PMMA A2 (M_w = 495,000 Da, Spectrochem) resist and 0.2 ml of anhydrous anisole (99.7% pure; Sigma-Aldrich) that was sonicated for half an hour to ensure proper mixing. The solutions are directly used for spin coating onto the Ge-coated (5 nm) metallic Ag (100 nm) mirrors. For thickness optimization, the solutions are first spin-coated at different revolutions per minute on clean microscopic glass slides, following which the films are annealed at a very low temperature of around 50°C for 5 min and are subsequently characterized for thickness measurements using a stylus profilometer (Bruker DektakXT).

For preparing cavity samples, Si (111) substrates are first cleaned by ultrasonication (3 min in each solvent) using acetone, methanol, and isopropanol as solvents. The steps are repeated thrice to ensure proper cleaning followed by drying with N$_2$ gun. Onto these cleaned Si (111) substrates, 5 nm of Ge is first deposited as an adhesive layer using electron beam (E-beam; AJA Orion 8E) evaporator at a slow deposition rate of 0.3 Å/s, following which 100 nm of Ag is deposited at a constant rate of 0.5 Å/s to form the bottom metallic mirror. The as-prepared DCS precursor solution is then properly filtered using a syringe filter and then spin-coated on these bottom Ag mirrors at 4000 and 4500 rpm for 1 min. The films are annealed at a very low temperature of around 50°C for 5 min to form the noncavity samples. The cavity samples are prepared in an exactly similar manner, following which 30 nm of top Ag mirror is directly deposited using E-beam at a constant rate of 0.3 Å/s. The same procedure is carried out with PMMA A2 resist only to prepare the bare cavity samples.

Optical and spectroscopic measurements
The reflection measurements are performed using spectroscopic ellipsometry (Woollam V-VASE) technique for all samples. For the bare film and cavity samples, reflection measurements are performed using the pp polarization by varying the angle of incident light from 20° to 50°. The measurements are collected at room temperature for each 5° interval. Solid-state UV-visible measurements on glass slides are performed using a Jasco-760 UV-visible spectrophotometer. PL measurements are performed using a homemade setup comprising laser. The setup is coupled with a Princeton Instruments monochromator with a PIXIS: 256 electron-multiplying

charge-coupled device (EMCCD) camera. A 100×, 0.7 numerical aperture (NA) objective was used for all the measurements.

Confocal Raman measurements

Raman spectra are recorded by raster-scanning the samples using a confocal Raman microscope (alpha300 R; WITec GmbH, Ulm, Germany). The system is equipped with an SHG Nd:yttrium-aluminum-garnet red laser (532 nm, 70 mW) and a lens-based spectrometer with a CCD camera (1024 × 128 pixel; Peltier cooled to ~65°C). A 100× microscope objective (working distance, 0.3 mm; 1.0 NA) was used for the experiments. The spectra are recorded as large-area scans with an integration time of 0.5 s at a laser power of ~9.0 mW measured at the microscope objective followed by averaging. The laser exposition time is first varied and then fixed to 13 min to examine the consistency (stability) of the spectral features, which is averaged and baseline corrected. All the spectra are corrected by subtracting the results obtained from the control samples consisting of PMMA films (no DCS) only. For confocal imaging, the 50-μm core of a multimode fiber served as the pinhole, leading to a focal depth of ~1 μm. The diffraction-limited spot resulted in a lateral resolution of ~1 to 2 μm. Reflected and elastically scattered photons were rejected by an edge filter. The nominal spectral resolution was ~5 cm^{-1} per CCD pixel. All measurements are done at room temperature.

DFT calculations

All calculations are performed using the Gaussian 16 suite of programs (40). The DCS geometry optimization is performed using MP2/6-31G(d). The absence of imaginary frequencies confirmed the optimized geometry as minima. Vibrational Raman spectra are obtained using the same level of theory. Molecular models are obtained using PyMOL 13.0 software.

SUPPLEMENTARY MATERIALS

Supplementary material for this article is available at https://science.org/doi/10.1126/sciadv.abj0997

REFERENCES AND NOTES

1. B. Zietz, E. Gabrielsson, V. Johansson, A. M. el-Zohry, L. Sun, L. Kloo, Photoisomerization of the cyanoacrylic acid acceptor group—A potential problem for organic dyes in solar cells. *Phys. Chem. Chem. Phys.* **16**, 2251–2255 (2014).
2. M. Irie, T. Fukaminato, K. Matsuda, S. Kobatake, Photochromism of diarylethene molecules and crystals: Memories, switches, and actuators. *Chem. Rev.* **114**, 12174–12277 (2014).
3. R. P. Sinha, D. P. Häder, UV-induced DNA damage and repair: A review. *Photochem. Photobiol. Sci.* **1**, 225–236 (2002).
4. J. A. Hutchison, T. Schwartz, C. Genet, E. Devaux, T. W. Ebbesen, Modifying chemical landscapes by coupling to vacuum fields. *Angew. Chem. Int. Ed.* **51**, 1592–1596 (2012).
5. J. Galego, F. J. Garcia-Vidal, J. Feist, Cavity-induced modifications of molecular structure in the strong-coupling regime. *Phys. Rev. X* **5**, 041022 (2015).
6. F. Herrera, F. C. Spano, Cavity-controlled chemistry in molecular ensembles. *Phys. Rev. Lett.* **116**, 238301 (2016).
7. K. Bennett, M. Kowalewski, S. Mukamel, Novel photochemistry of molecular polaritons in optical cavities. *Faraday Discuss.* **194**, 259–282 (2016).
8. B. Munkhbat, M. Wersäll, D. G. Baranov, T. J. Antosiewicz, T. Shegai, Suppression of photo-oxidation of organic chromophores by strong coupling to plasmonic nanoantennas. *Sci. Adv.* **4**, eaas9552 (2018).
9. J. Feist, J. Galego, F. J. Garcia-Vidal, Polaritonic chemistry with organic molecules. *ACS Photonics* **5**, 205–216 (2018).
10. R. F. Ribeiro, L. A. Martínez-Martínez, M. Du, J. Campos-Gonzalez-Angulo, J. Yuen-Zhou, Polariton chemistry: Controlling molecular dynamics with optical cavities. *Chem. Sci.* **9**, 6325–6339 (2018).
11. A. Mandal, P. Huo, Investigating new reactivities enabled by polariton photochemistry. *J. Phys. Chem. Lett.* **10**, 5519–5529 (2019).
12. D. M. Coles, N. Somaschi, P. Michetti, C. Clark, P. G. Lagoudakis, P. G. Savvidis, D. G. Lidzey, Polariton-mediated energy transfer between organic dyes in a strongly coupled optical microcavity. *Nat. Mater.* **13**, 712–719 (2014).
13. X. Zhong, T. Chervy, S. Wang, J. George, A. Thomas, J. A. Hutchison, E. Devaux, C. Genet, T. W. Ebbesen, Non-radiative energy transfer mediated by hybrid light-matter states. *Angew. Chem. Int. Ed.* **55**, 6202–6206 (2016).
14. R. Saez-Blazquez, J. Feist, A. I. Fernandez-Dominguez, F. J. Garcia-Vidal, Organic polaritons enable local vibrations to drive long-range energy transfer. *Phys. Rev. B* **97**, 241407 (2018).
15. G. Groenhof, J. J. Toppari, Coherent light harvesting through strong coupling to confined light. *J. Phys. Chem. Lett.* **9**, 4848–4851 (2018).
16. M. Du, L. A. Martínez-Martínez, R. F. Ribeiro, Z. Hu, V. M. Menon, J. Yuen-Zhou, Theory for polariton-assisted remote energy transfer. *Chem. Sci.* **9**, 6659–6669 (2018).
17. A. M. Berghuis, A. Halpin, Q. Le-Van, M. Ramezani, S. Wang, S. Murai, J. Gómez Rivas, Enhanced delayed fluorescence in tetracene crystals by strong light-matter coupling. *Adv. Funct. Mater.* **29**, 1901317 (2019).
18. M. Wang, M. Hertzog, K. Börjesson, Polariton-assisted excitation energy channeling in organic heterojunctions. *Nat. Commun.* **12**, 1874 (2021).
19. Y. Yu, S. Mallick, M. Wang, K. Börjesson, Barrier-free reverse-intersystem crossing in organic molecules by strong light-matter coupling. *Nat. Commun.* **12**, 3255 (2021).
20. F. J. Garcia-Vidal, C. Ciuti, T. W. Ebbesen, Manipulating matter by strong coupling to vacuum fields. *Science* **373**, eabd0336 (2021).
21. S. Haroche, D. Kleppner, Cavity quantum electrodynamics. *Phys. Today* **42**, 1, 24–30 (1989).
22. V. M. Agranovich, A. G. Malshukov, Surface polariton spectra if the resonance with the transition layer vibrations exist. *Optics Comm.* **11**, 169–171 (1974).
23. I. Pockrand, A. Brillante, D. Möbius, Exciton–surface plasmon coupling: An experimental investigation. *J. Phys. Chem.* **77**, 6289–6295 (1982).
24. D. G. Lidzey, D. D. C. Bradley, M. S. Skolnick, T. Virgili, S. Walker, D. M. Whittaker, Strong exciton–photon coupling in an organic semiconductor microcavity. *Nature* **395**, 53–55 (1998).
25. F. D. Lewis, W. Weigel, Excited state properties of donor–acceptor substituted trans-stilbenes: The meta-amino effect. *J. Phys. Chem. A* **104**, 8146–8153 (2000).
26. M. Albota, D. Beljonne, J. L. Brédas, J. E. Ehrlich, J. Y. Fu, A. A. Heikal, S. E. Hess, T. Kogej, M. D. Levin, S. R. Marder, D. McCord-Maughon, J. W. Perry, H. Röckel, M. Rumi, G. Subramaniam, W. W. Webb, X. L. Wu, C. Xu, Design of organic molecules with large two-photon absorption cross sections. *Science* **281**, 1653–1656 (1998).
27. J. E. Ehrlich, X. L. Wu, I. Y. S. Lee, Z. Y. Hu, H. Röckel, S. R. Marder, J. W. Perry, Two-photon absorption and broadband optical limiting with bis-donor stilbenes. *Opt. Lett.* **22**, 1843–1845 (1997).
28. J. H. Strickler, W. W. Webb, Three-dimensional optical data storage in refractive media by two-photon point excitation. *Opt. Lett.* **16**, 1780–1782 (1991).
29. W. Denk, Two-photon scanning photochemical microscopy: Mapping ligand-gated ion channel distributions. *Proc. Nat. Acad. Sci. U.S.A.* **91**, 6629–6633 (1994).
30. W.-G. Han, T. Lovell, T. Liu, L. Noodleman, Density functional studies of the ground- and excited-state potential-energy curves of stilbene cis–trans isomerization. *ChemPhysChem* **3**, 167–178 (2002).
31. B. P. Kar, N. Ramanathan, K. Sundararajan, K. S. Viswanathan, Matrix isolation FTIR studies of non-planar trans-stilbene. *J. Mol. Str.* **994**, 364–370 (2011).
32. M. Edelson, A. Bree, The geometry of trans-stilbene in the liquid phase. *Chem. Phys. Lett.* **41**, 562–564 (1976).
33. M. Traetteberg, E. B. Frantsen, F. C. Mijlhoff, A. Hoekstra, A gas electron diffraction study of the molecular structure of trans-stilbene. *J. Mol. Str.* **26**, 57–68 (1975).
34. E. Abraham, J. Oberlé, G. Jonusauskas, R. Lapouyade, C. Rullière, Dual excited states in 4-dimethylamino 4′-cyanostilbene (DCS) revealed by sub-picosecond transient absorption and Kerr ellipsometry. *J. Photochem. Photobiol. A Chem.* **105**, 101–107 (1997).
35. M. Borowiak, B. Grobelna, A. Synak, P. Bojarski, A. A. Kubicki, Time-resolved emission spectra of 4-dimethylamino-4′-cyano-stilbene and resveratrol in high viscosity solvents and silica matrices. *Spectrochim. Acta A Mol. Biomol. Spectros.* **115**, 111–117 (2013).
36. S. Baieva, O. Hakamaa, G. Groenhof, T. T. Heikkilä, J. J. Toppari, Dynamics of strongly coupled modes between surface plasmon polaritons and photoactive molecules: the effect of the Stokes shift. *ACS Photonics* **4**, 28–37 (2017).
37. J. A. Guicheteau, A. Tripathi, E. D. Emmons, S. D. Christesen, A. W. Fountain III, Reassessing SERS enhancement factors: Using thermodynamics to drive substrate design. *Faraday Discuss.* **205**, 547–560 (2017).
38. I. Persaud, W. E. L. Grossman, Surface-enhanced Raman scattering of triphenylmethane dyes on colloidal silver. *J. Raman Spect.* **24**, 107–112 (1993).
39. G. Groenhof, C. Climent, J. Feist, D. Morozov, J. J. Toppari, Tracking polariton relaxation with multiscale molecular dynamics simulations. *J. Phys. Chem. Lett.* **10**, 5476–5483 (2019).

40. M. J. Frisch, G. W. Trucks, H. B. Schlegel, G. E. Scuseria, M. A. Robb, J. R. Cheeseman, G. Scalmani, V. Barone, G. A. Petersson, H. Nakatsuji, X. Li, M. Caricato, A. V. Marenich, J. Bloino, B. G. Janesko, R. Gomperts, B. Mennucci, H. P. Hratchian, J. V. Ortiz, A. F. Izmaylov, J. L. Sonnenberg, D. Williams-Young, F. Ding, F. Lipparini, F. Egidi, J. Goings, B. Peng, A. Petrone, T. Henderson, D. Ranasinghe, V. G. Zakrzewski, J. Gao, N. Rega, G. Zheng, W. Liang, M. Hada, M. Ehara, K. Toyota, R. Fukuda, J. Hasegawa, M. Ishida, T. Nakajima, Y. Honda, O. Kitao, H. Nakai, T. Vreven, K. Throssell, J. A. Montgomery, Jr., J. E. Peralta, F. Ogliaro, M. J. Bearpark, J. J. Heyd, E. N. Brothers, K. N. Kudin, V. N. Staroverov, T. A. Keith, R. Kobayashi, J. Normand, K. Raghavachari, A. P. Rendell, J. C. Burant, S. S. Iyengar, J. Tomasi, M. Cossi, J. M. Millam, M. Klene, C. Adamo, R. Cammi, J. W. Ochterski, R. L. Martin, K. Morokuma, O. Farkas, J. B. Foresman, and D. J. Fox, Gaussian 16 C.01, Gaussian, Inc., Wallingford CT (2016).

Citation: S. Satapathy, M. Khatoniar, D. K. Parappuram, B. Liu, G. John, J. Feist, F. J. Garcia-Vidal, V. M. Menon, Selective isomer emission via funneling of exciton polaritons. *Sci. Adv.* **7**, eabj0997 (2021).

Science Advances

Selective isomer emission via funneling of exciton polaritons

Sitakanta SatapathyMandeep KhatoniarDivya K. ParappuramBin LiuGeorge JohnJohannes FeistFrancisco J. Garcia-VidalVinod M. Menon

View the article online
https://www.science.org/doi/10.1126/sciadv.abj0997
Permissions
https://www.science.org/help/reprints-and-permissions

Use of think article is subject to the Terms of service